TRIANGULAR BROAD CRESTED WEIR THEORY AND EXPERIMENT

ACHOUR B.[1]*, AMARA L.[2]

[1] Professor, Research laboratory in subterranean and surface hydraulics (LARHYSS), University of Biskra, Algeria
[2] Associate Professor, Department of Civil Engineering and Hydraulics, Faculty of Science and Technology, University of Jijel, Algeria

[*] *bachir.achour@larhyss.net*

ABSTRACT

The article looked at the possibility of making use of a triangular broad crested device, provided with a crest height P and a constant apex angle θ, as a flow measurement weir. The device has a triangular gorge which extends over a certain length L. This must be sufficient to allow the creation of a control section in a given section of the gorge, which represents the prerequisite condition for the proper functioning of the device. Inserted in a rectangular channel of width B for which the measurement of the flow rate Q is needed, the device causes a lateral contraction of the cross section located above the crest height P. It is shown that the dimensionless parameter $M_1 = mh_1/B$ reflects the effect of this lateral contraction, where $m = tg(\theta/2)$, and h_1 is the upstream flow depth counted above the crest. Due to the crest height P, the flow also undergoes vertical contraction. The effect of both lateral and vertical contractions can be grouped together in a single dimensionless parameter noted ψ such that $\psi = M_1/(1+P^*)$ where $P^* = P/h_1$ denotes the relative crest height.

After the detailed description of the device as well as the resulting flow, a dimensional analysis has been proposed in order to identify the parameters on which the discharge coefficient C_d of the device depends. It has been clearly demonstrated that the flow coefficient can be written as a function of both M_1 and P^*, i.e. $C_d = \lambda(M_1, P^*)$.

In order to define the function λ, a theoretical approach is proposed based on the momentum theorem and the energy equation. This approach turned out to be judicious since it led to expressing the theoretical relationship that governs the discharge coefficient

C_d. This was presented as an explicit function of the dimensionless parameter ψ, depending therefore on both M_1 and P^* as predicted by dimensional analysis.

After that, experimental tests were rigorously carried out on six devices with different geometric characteristics. The objective was to verify the validity of the theoretical relationship governing the discharge coefficient. The tests were carried out under suitable hydraulic conditions and the flow rate Q and the upstream depth h_1 were measured using high precision instruments. In total, 122 measurement points were collected and were carefully analyzed. The use of linear least-squares fitting method involving experimental and theoretical data gave the following trend line relationship:

$$C_{d,Exp} = 0.9999\, C_{d,Th} \approx C_{d,Th}$$

It was thus concluded that the theoretical discharge coefficient relationship did not need any correction and it could be used with great confidence since the maximum deviation observed rarely reached 0.2%. This is also the case for the relationship that governs the flow rate Q.

Keywords: Flow measurement, Triangular broad-crested weir, theoretical approach, discharge coefficient.

INTRODUCTION

It is universally known that the flow measurement in open channels is essentially based on establishing the Depth–discharge law commonly called "Stage-discharge" relationship. Knowing the geometric characteristics of the device, the flow rate is then calculated using this law after having measured the flow upstream of the device. When the calculated flow rate depends both on the geometry of the device and on the upstream flow depth, the device is then called "semi-modular" (Achour, 2003). This is generally the case with all devices used for measuring the flow rate in open channels, with the exception of siphons which are modular. One of the most famous devices of its time was the "Neyrpic mask module", also called "Neyrpic modular siphon" (Carlier, 1998). The flow rate that is conveyed depends only on the geometric characteristics of the device, independent of fluctuations in the upstream level of the flow. This means that for an already designed device, of given geometry, the delivered flow rate is constant. These devices are completely static and their properties depend on the association of a profiled sill and an inclined mask, placed in such a way that they compensate for the effect of rising water level. However, this device is no longer used today although there are still a few specimens in operation worldwide.

The stage-discharge relationship is most often determined by laboratory testing through what is commonly referred to as "Instrument calibration". The tests make it possible to deduce a curve, generally of power form, of type $Q = ah^b$ called a calibration curve which can be plotted in a logarithmic or in a Cartesian division coordinate system. The *Q-h*

relationship is specific to each device whose characteristics are contained in the constant "*a*". The calibration curve is then used to read the value of the flow rate *Q* when the upstream flow depth *h* is known. Other users prefer to translate this curve into a table of values which however often requires linear interpolations. The flow rate tables values contained in the ISCO Open Channel Flow Measurement Handbook (Teledyne ISCO, 2021), eighth or later edition, or those provided by the manufacturer, are examples of tools that can be used for this purpose.

The means of measuring the flow rate differ depending on whether the flow takes place in pipes or in open channels. But the something in common lies in the fact that the flow measurement is based on the principle of a flow contraction either vertical or lateral, and sometimes even both (Bos, 1976; Achour et al., 2003; Achour and Amara, 2021). This is the case with open channels that interests the present study and to which all due attention will be paid.

Devices that use the property of a vertically contracted flow are those that have a crest height that the flow crosses. These are devices that are called "suppressed weirs" devoid of end contraction such that the crest is running all the way across the width of the channel so the head loss will be negligible. The geometric and hydraulic properties of such structures are detailed in specialized literature (SIA, 1926; Henderson, 1966; Achour et al., 2003).

On the other hand, the devices which are the seat of both a lateral and a vertical contraction of the flow are called "Contracted weirs" endowed with an end contraction and a crest height as well (Bos, 1976; Achour et al., 2003; Vatankhah and Khamisabadi, 2019). Due to the end contraction, they have a central opening which can be rectangular (rectangular weir), triangular (triangular weir) or trapezoidal shape (trapezoidal weir) allowing the crossing of the flow (Bos, 1976; 1989; Hager, 1986; Achour et al., 2003).

Devices which take advantage on the property of a laterally contracted flow are devoid of crest height. They are designed in such a way that their geometry causes a lateral reduction of the flow crossing section. They can be composed of two thin plates placed across the flow on either side of the walls of the channel, allowing the flow to pass through a central opening. This is a sharp-edged width constriction which is the simplest configuration that can be conceived for a measuring flow device in open channels (Achour and Amara, 2021).

Moreover, devices which only cause lateral contraction of the flow are obviously devoid of crest height but are designed with a broad wall extending over a certain length *L*. This length should be sufficient for a control section to be created into a given section of the gorge because this is the prerequisite condition for the proper functioning of the device (Achour et Amara, 2022).

The flow rate in open channels can also be measured using what are called "Hydraulic jump gauges", depending on field condition. The best known are the Parshall and the Venturi (Bos, 1976; 1989; Achour et al., 2003) and a little less used the modified Venturi (Hager, 1985). The design adopted for these devices is such that the flow passes through

a control section, followed by short slice of supercritical flow before the formation of the hydraulic jump. The presence of a hydraulic jump is an advantage since it makes it possible to raise the downstream body of water, which is desired above all when the slopes are low (Achour, 1989). In the control section, the corresponding critical depth is closely related to the flow rate to be measured. With the exception of the hydraulic jump gauge proposed by Achour in 1989, which is of triangular cross-section, all the other known hydraulic jump gauges are of rectangular cross-section.

With regard to this study, it is on a broad-crested configuration that will focus all the required attention, with in addition that the device is provided with a crest height P. The flow should therefore experience the combined effect of lateral and vertical contractions. In fact, this is a broad-crested device provided with a crest height P, consisting of a triangular cross-section the gorge of which extends over a given length L. One of the attracting advantages of such a device is that the triangular section allows excellent accuracy for both high and low flow rates. This is not the case with the rectangular cross-section for which acceptable precision in the measurement of the flow rate is only obtained for high flow depths. However, the existence of a crest height, like a barrier, is not advantageous insofar as the device no longer has the self-cleaning property. Indeed, solid debris carried by the flow coming from the upstream are likely to accumulate in front of the device for which regular cleaning is then necessary.

What is expected is to subject the device to a thorough investigation as theoretical as experimental. The theory is expected to explain experimental results and to predict new results, while experiment is expected to check the validity of the theory and to gather and manage data for possibly modifying it. What one wishes to achieve at the end of the theoretical development is to establish the relationship that governs the flow rate. This relation should especially take into account the effect of the approach flow velocity which is an important flow rate influencing factor. It is also envisioned to write the theoretical flow rate relationship in the known form governing the triangular weir in order to extract the general expression of the discharge coefficient. It is this relationship that will be subjected to an intense experimental program in order to confirm its validity or to possibly correct it if deviations will be observed between experimental and theoretical values.

MATERIAL AND METHODS

Description of the device and the flow

Fig. 1 shows a perspective representation of the apparatus placed in an approach channel of rectangular cross-section of width B. It consists over its entire length L of a triangular cross-section with a constant opening angle θ. In addition, its height is h_0 equal to that of the channel and it is in particular endowed with a crest height P. The flow rate conveyed by the channel is noted Q while h_1 designates the upstream flow depth counted above the crest, i.e. above the vertex of the triangle.
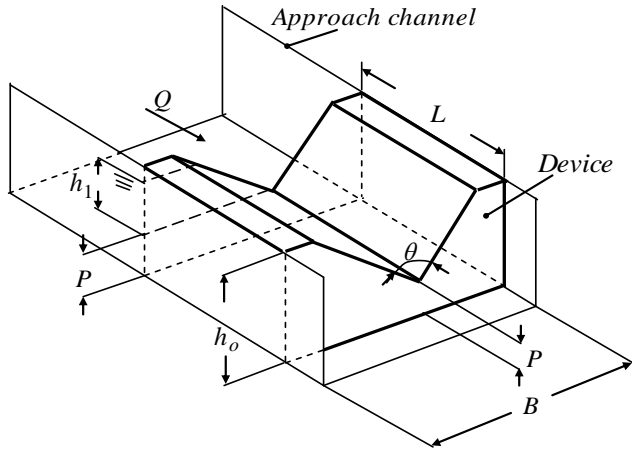
Figure 1: Perspective view of the device settled in a rectangular approach channel

Fig. 2 clearly shows the device in a front view when it is in the dry state before its operation, whilst Fig. 3 illustrates the device in operation seen from downstream. It can easily be seen that the flow upstream of the device is calm and quiet, showing no appreciable disturbance of the free surface. This state is well confirmed by Fig. 4.

The geometric forms of the device thereby generate two contractions of the flow. The first contraction is lateral due to the change from the upstream rectangular section to a reduced triangular section at the entrance of the device. Indeed, the cross-section decreases from the quantity Bh_o corresponding to the rectangular channel cross-section to mh_o^2 representing the triangular cross-section, where $m = tg(\theta/2)$. The second one is vertical since the device is endowed with a crest height of *P*.
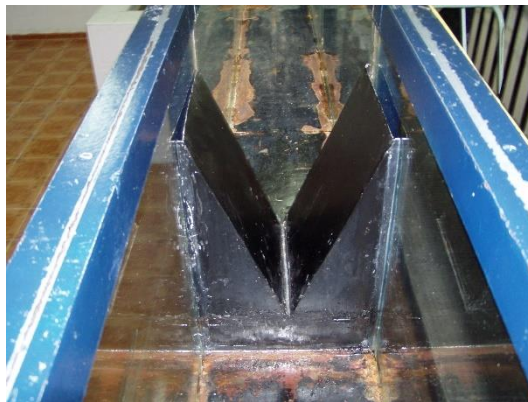

Figure 2: The device in the dry state placed in a rectangular channel

Figure 3: View of the downstream side of the device in operation

Figure 4: View of the flow upstream and downstream of the device. Flow from right to left.

It is worth noting that the maximal depth above the crest is (Fig. 1):

$$h_{1,\max} = h_o - P \tag{1}$$

This particularity corresponds to the following:

$$m = tg(\theta_{\max}/2) = \frac{B/2}{h_{1,\max}} = \frac{B}{2(h_o - P)} \tag{2}$$

Considering the following dimensionless parameter:

$$M_1 = \frac{m\,h_1}{B} \tag{3}$$

it is then easy to show when referring to Eq. (2), that the maximal value of M_1 is as:

$$M_{1,\max} = \frac{m\, h_{1,\max}}{B} = \frac{1}{2} \tag{4}$$

On the other hand, for low values of the depth above the crest or for large values of the width B of the approach channel, one may write $M_1 \to 0$ in accordance with Eq. (3). Taking these considerations into account, it is justifiable to write that:

$$0 \le M_1 \le 1/2 \tag{5}$$

The physical meaning of parameter M_1 becomes clearer when one write what follows:

$$M_1 = \frac{m\, h_1}{B} = \frac{m\, h_1^2}{B\, h_1} = \frac{\text{Contracted triangular section}}{\text{Rectangular section above the crest}} \tag{6}$$

It is therefore a parameter that reflects the effect of the contraction of the cross-section of the supply channel located above the height crest P. In addition, the effect of the transverse contraction of the entire supply section of the channel, located upstream of the device, can be reflected in the following dimensionless parameter:

$$\psi = \frac{m\, h_1^2}{B\,(h_1 + P)} \tag{7}$$

Eq. (7) can be rewritten as:

$$\psi = \frac{M_1}{1 + P^*} \tag{8}$$

where P^* is the relative crest height defined as:

$$P^* = \frac{P}{h_1} \tag{9}$$

The smallest value that could take by the dimensionless parameter ψ is zero and corresponds either to $M_1 \to 0$ or to large values of the relative crest height P^*, i.e. $P^* \to \infty$. On the other hand, the maximum value of ψ is obtained for the low values of the relative crest height P^*, i.e. $P^* \to 0$, and for the largest value of M_1 as well, i.e. $M_{1,\max} = 1/2$. It is therefore obvious to write that:

$$0 \le \psi \le 1/2 \tag{10}$$

In the next sections, it will be demonstrated the important role that the dimensionless parameter ψ plays in the flow rate and discharge coefficient relationships.

Regarding the flow, Fig. 5 shows the longitudinal profile revealing a subcritical flow in the upstream section 1-1 and supercritical inside the throat of the apparatus. The changeover from the subcritical flow to the supercritical flow results in the occurrence of a control section c-c where the flow depth is critical symbolized by h_c. The existence of a critical regime within the gorge is the first and *sine qua non* condition for the correct functioning of the device as a flowmeter as long as the length L is sufficient for the emerging of a control section. The longitudinal profile shown in Fig. 5 has been observed experimentally for all the tested devices for which the chosen length L was sufficient.

For the case of a triangular section, the critical depth h_c is written as:

$$h_c = \left(\frac{2 Q^2}{g \, m^2} \right)^{1/5} \tag{11}$$

where g is the acceleration due to gravity.
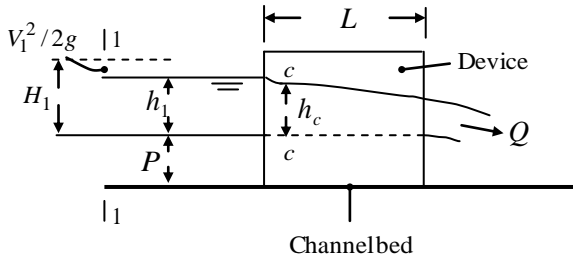
Figure 5: Longitudinal profile of the flow upstream and within the device

The total upstream head above the crest, defined as H_1 (Fig. 5), is governed by the following relationship:

$$H_1 = h_1 + \frac{V_1^2}{2g} \tag{12}$$

where V_1 denotes the mean flow velocity. Noting A_1 as the water area in section 1-1, the mean flow velocity V_1 is given by the ratio Q/A_1 where A_1 can be written as:

$$A_1 = B\left(h_1 + P \right) \tag{13}$$

Thus, Eq. (12) reduces to:

$$H_1 = h_1 + \frac{Q^2}{2g \, B^2 \, (h_1 + P)^2} \tag{14}$$

Eq. (14) can be rewritten as:

$$H_1 = \left[1 + \frac{Q^2}{2g\,B^2 h_1\,(h_1 + P)^2}\right]h_1 \tag{15}$$

It thus appears that the total head H_1 can be written in the following form:

$$H_1 = (1 + \delta)h_1 \tag{16}$$

where δ is a kinetic factor defined as:

$$\delta = \frac{Q^2}{2g\,B^2 h_1\,(h_1 + P)^2} \tag{17}$$

In other words, it amounts to writing that $\delta \times h_1 = V_1^2/2g$ thus reflecting the fact that the approach velocity head is a fraction δ of the upstream depth h_1. It is self-evident that the kinetic factor δ is less than unity, varying within the range $0 \leq \delta < 1$. On may even show that δ is equal to ½ in the case of critical flow. For the case where $\delta \rightarrow 0$, the approach flow velocity is then insignificant implying that the total head H_1 can be assimilated to the upstream depth h_1 in accordance with Eq. (16).

It will be seen in an appropriate section that Eq. (17) will play a momentous role in taking into account the approach flow velocity when deriving the theoretical relationship governing the flow rate passing through the device.

Dimensional analysis and discharge coefficient dependency

Through a qualitative functional relationship, the dimensional analysis allows highlighting the parameters on which the discharge coefficient C_d of the device depends. One may logically enumerate the ten physical parameters involved in the current problematic namely: the discharge Q, the upstream depth h_1 counted over the crest, the crest height P, the channel width B, the apex angle θ, the crest length L, the acceleration due to gravity g, the density of the flowing liquid ρ, the dynamic viscosity μ of the liquid, and the surface tension σ. These parameters are interrelated by the following functional relationship:

$$f\left(Q, \rho, g, h_1, B, L, \mu, \sigma, \theta\right) = 0 \tag{18}$$

Using Vashy-Buckingham π theorem (Langhaar, 1951), the stage-discharge relationship as function of dimensionless parameters can be derived as follows:

$$Q = g^{1/2} h_1^{5/2} \phi \left(\frac{\rho \, g^{1/2} h_1^{3/2}}{\mu}, \frac{\rho g h_1^2}{\sigma}, \frac{h_1}{L}, \frac{h_1}{B}, \frac{h_1}{P}, \theta \right) \tag{19}$$

ϕ denotes the function symbol expressing the discharge coefficient C_d relationship. One can notice that the first and the second quantities between the brackets correspond to the Reynolds number R_e and the Weber number W_e respectively. Consequently, the discharge coefficient C_d is functionally written as follows:

$$C_d = \phi \left(R_e, W_e, \frac{h_1}{L}, \frac{h_1}{B}, \frac{h_1}{P}, \theta \right) \tag{20}$$

It is worth noting that given the turbulent nature of the flow, the effect of the Reynolds number R_e is not at all significant. In addition, the effect of the surface tension expressed by the Weber number W_e only appears for low flow rates Q and for small values of the apex angle θ, that is to say for a tightened throat case. On the other hand, the influence of the length L can be neglected provided that the ratio L/h_1 exceeds the threshold value defining the broad crested criteria.

Taking all these considerations into account and considering $m = tg(\theta/2)$, Eq. (20) reduces to:

$$C_d = \lambda \left(\frac{h_1}{B}, \frac{h_1}{P}, m \right) \tag{21}$$

On the other hand, combining the variables h_1/B and m, one can form the dimensionless parameter $M_1 = mh_1/B$ expressed by Eq. (3). Finally, Eq. (21) is written in its following final form:

$$C_d = \lambda \left(M_1, P^* \right) \tag{22}$$

Recall that P^* is defined by Eq. (9) as $P^* = P/h_1$. The λ functional relationship will be theoretically defined in the next sections through the use of both momentum and energy equations.

One of the simplified geometric configurations is that corresponding to a device devoid of crest height, i.e. $P = 0$ or $P^* = 0$. In accordance with Eq. (22), the discharge coefficient for such a particular geometry depends solely on the dimensionless parameter $M_1 = mh_1/B$. Besides, this has been theoretically demonstrated by the authors in a recent study (Achour and Amara, 2022).

Theoretical relative depth and relative head relationships

For the rest of the study, let us define the relative depth h_1^* as being the ratio between the upstream depth h_1 over the crest and the critical depth h_c in the section c-c inside the triangular gorge (Fig. 5). Thus:

$$h_1^* = \frac{h_1}{h_c} \tag{23}$$

It is worth noting that the relative depth h_1^* is greater than unity since the upstream depth h_1 is greater than the critical depth h_c. This can besides be observed in Fig. 5.

Expressing the relationship which governs the relative depth h_1^* is fundamental for the theoretical development. For this, the resort to the momentum theorem, applied between two well-chosen sections of the flow, turns out to be very useful. The two sections involved are sections 1-1 and c-c shown in Fig. 5. However, it is agreed to allow some simplifying assumptions when applying the momentum equation, which are as follows: the pressure distribution is assumed to be hydrostatic in any section of the flow, whether in the supply channel or inside the device; the velocity distribution is assumed to be uniform in the chosen sections; the friction loss is assumed to be negligible over the short distance separating the two selected sections; the air resistance is negligible, and the effect of the streamline curvature is also neglected.

The momentum equation translates that the variation in the quantity $\rho Q V$ between the sections involved is equal to the sum of all the external forces which apply to these same sections. These forces must above all be projected onto a longitudinal axis, the direction of which is often that of flow. Let us define before that the following parameters namely: $V_c = Q / A_c$ the critical velocity at section c-c (Fig. 5); F_c the pressure force acting on section c-c of cross-sectional area A_c; F_1 the pressure force acting on section 1-1 of cross-sectional area A_1; F_R the reaction force acting on the upstream side of the device of involved surface area A_R. One may write rightly what follows:

$$F_1 = \rho g \overline{h_1} A_1 \tag{24}$$

where $\overline{h_1}$ is the depth at the centroid of the cross-sectional area A_1 counted from the free surface flow. As section 1-1 is located in the rectangular part upstream of the device (Fig. 5), and then one may write the following equations:

$$\overline{h_1} = \frac{h_1 + P}{2} \tag{25}$$

$$A_1 = B(h_1 + P) \tag{26}$$

In the same form as Eq. (24), one can write the pressure force F_c as:

$$F_c = \rho g \overline{h_c} A_c \tag{27}$$

where $\overline{h_c}$ is the depth at the centroid of the critical cross-sectional area A_c counted from the free surface flow. The section c-c (Fig. 5) being triangular, one may write what follows:

$$\overline{h_c} = \frac{h_c}{3} \tag{28}$$

and

$$A_c = m h_c^2 \tag{29}$$

In the same way, the reaction force F_R can be written in the following form:

$$F_R = \rho g \overline{h_R} A_R \tag{30}$$

where:

$$\overline{h_R} = \frac{(h_1 + P)}{6} \left[\frac{3B - 2m(h_1 + P)}{B - m(h_1 + P)} \right] \tag{31}$$

$$A_R = B(h_1 + P) - m h_1^2 \tag{32}$$

Application of the momentum equation in the longitudinal direction yields:

$$\rho Q (V_c - V_1) = F_1 - F_c - F_R \tag{33}$$

Replacing in Eq. (33) parameters by their respective expression and after making some simplifications and rearrangements, it follows that:

$$h_1^{*5} - \frac{5}{2} h_1^{*2} + \frac{3}{2} \frac{M_1}{(1 + P^*)} = 0 \tag{34}$$

Eq. (34) clearly shows that the relative depth h_1^* depends on both the dimensionless parameters $M_1 = m h_1 / B$ and $P^* = P / h_1$.

Taking into account Eq. (8), Eq. (34) reduces to:

$$h_1^{*5} - \frac{5}{2} h_1^{*2} + \frac{3}{2} \psi = 0 \tag{35}$$

It is useful to remember that $0 \le \psi \le \tfrac{1}{2}$ and $h_1^* > 1$.

The graphic representation of Eq. (35) shows that h_1^* decreases with increasing ψ. Let us note two particular values resulting from Eq. (34):

$$h_1^*(\psi = 0) = 1.3572$$

and

$$h_1^*(\psi = 1/2) = 1.2667$$

One can therefore conclude that when ψ varies in the range [0; 0.5]. The relative depth h_1^* extends between the following extreme values: 1.2667 and 1.3572.

As for the relative depth, the relative total head is defined as being the ratio between the upstream total head H_1 above the crest (Fig. 5) and the critical depth h_c inside the device in section c-c. That is:

$$H_1^* = \frac{H_1}{h_c} \tag{36}$$

Dividing both sides of Eq. (14) by h_c yields:

$$H_1^* = h_1^* + \frac{Q^2}{2g\,B^2\,h_c\,(h_1 + P)^2} \tag{37}$$

On the other hand, eliminating the discharge Q between Eqs. (11) and (37) results in:

$$H_1^* = h_1^* + \frac{g\,m^2\,h_c^5}{4g\,B^2\,h_c\,(h_1 + P)^2} \tag{38}$$

After performing some transformations, Eq. (38) reduces to:

$$H_1^* = h_1^* + \frac{M_1^2}{4\,h_1^{*4}\,(1 + P/h_1)^2} \tag{39}$$

Eq. (39) can be simply rewritten as:

$$H_1^* = h_1^* + \frac{\psi^2}{4\,h_1^{*4}} \tag{40}$$

As is Eq. (35), Eq. (40) is implicit in h_1^*. However, what is of interest to point out is the fact that H_1^* depends solely on ψ in accordance with both Eqs. (35) and (40). To avoid tedious calculations resulting from the simultaneous application of Eqs. (35) and (40), an

in-depth examination based on linear correlation analysis allowed deriving the following explicit $H_1^{*-1}(\psi)$ relationship:

$$H_1^{*-1} = \frac{h_c}{H_1} = 0.0768\,\psi + 0.7368 \tag{41}$$

Eq. (41) was obtained with a very convincing coefficient of determination, i.e. $R^2 = 0.9996$. In addition, the comparison between the approximate and exact values of H_1^{*-1}, computed using Eqs. (41) and (40) respectively, gave insignificant deviations. In fact, the maximum deviation observed in the whole aforementioned range values of ψ was only 0.078% obtained for the largest value $\psi = 0.5$.

Discharge and discharge coefficient relationships

The theoretical flow rate relationship must be established imperatively taking into account the effect of the approach flow velocity. This effect is theoretically reflected in Eq. (17). Combining Eqs. (11), (15), (17), and (41) yields:

$$Q = \frac{1}{2}\sqrt{2g}\, m\,(1+\delta)^{5/2}\,\zeta^{5/2}\,h_1^{5/2} \tag{42}$$

where the function ζ is governed by Eq. (41), that is to say:

$$\zeta(\psi) = 0.0768\,\psi + 0.7368 \tag{41a}$$

Inserting Eq. (42) into Eq. (17) and rearranging results in:

$$\delta = \frac{1}{4}\frac{M_1^2\,\zeta^5\,(1+\delta)^5}{(1+P/h_1)^2} \tag{43}$$

Let us define C_ψ as the following function exclusively dependent on ψ:

$$C_\psi = \psi\,\zeta^{5/2} \tag{44}$$

Consequently, Eq. (43) reduces to:

$$\delta = \frac{1}{4}C_\psi^2\,(1+\delta)^5 \tag{45}$$

It thus appears that the kinetic factor δ depends solely on ψ. It has been observed that throughout the range $0 \le \psi \le \frac{1}{2}$ the kinetic factor δ is much less than unity. Thus, as the result of a first order Taylor series expansion, it is relevant to write that $(1+\delta)^5 \approx 1+5\delta$. Inserting this result into Eq. (45) yields:

$$\delta = \frac{C_\psi^2}{4 - 5\,C_\psi^2} \tag{46}$$

It is thus derived the explicit delta relationship which quantifies the effect of the approach flow velocity. This effect depends on the value of ψ through the C_ψ function. The values of δ, grouped together in Table 1, clearly show that the effect of the approach flow velocity cannot be neglected, especially for large values of ψ.

Table 1: Values of the kinetic factor δ according to Eq. (46)

ψ	δ	$(1+\delta)^{5/2}$
0.10	0.00057339	1.00143409
0.15	0.00132872	1.00332512
0.20	0.00243675	1.00610301
0.25	0.0039345	1.0098653
0.30	0.00586608	1.01472979
0.35	0.00828438	1.0208398
0.40	0.01125336	1.02837129
0.45	0.01485108	1.03754227
0.50	0.01917377	1.04862592

As an illustrative example that allows affirming that the effect of the approach flow velocity cannot be neglected in all cases, let us consider for this the value $\psi = 0.40$. According to table 1, the kinetic factor δ is such that $\delta = 0.01125336$. The value of the quantity $(1+\delta)^{5/2}$ involved in Eq. (42) expressing the flow rate Q is given by Table 1 as $(1+\delta)^{5/2} = 1.05228911$. This result reveals that, for $\psi = 0.40$, if one were to neglect the approach flow velocity, more than 5.2% of error would be then committed in the calculation of the flow rate Q. This would be detrimental in certain practical cases for which such imprecision is not advisable.

Eq. (46) allows writing that:

$$(1+\delta)^{5/2} = \left(\frac{1 - C_\psi^2}{1 - \dfrac{5}{4}\,C_\psi^2} \right)^{5/2} \tag{47}$$

Thus, Eq .(42) is written as follows:

$$Q = \frac{1}{2}\sqrt{2g}\, m\left(\frac{1-C_\psi^2}{1-\frac{5}{4}C_\psi^2}\right)^{5/2} \zeta^{5/2}\, h_1^{5/2} \tag{48}$$

Eq. (48) is the first form of the stage-discharge relationship sought which can be written in the following reduced form usually assigned to triangular weirs:

$$Q = C_{d,1}\sqrt{2g}\, m\, h_1^{5/2} \tag{49}$$

where $C_{d,1}$ is the discharge coefficient expressed as:

$$C_{d,1} = \frac{1}{2}\left(\frac{1-C_\psi^2}{1-\frac{5}{4}C_\psi^2}\right)^{5/2} \zeta^{5/2} \tag{50}$$

Eq. (50) shows that the discharge coefficient depends solely on the dimensionless parameter ψ which is connected to the two variables M_1 and P^* according to explicit Eq. (8). According to this equation, the particular case where $\psi \to 0$ corresponds either to $M_1 \to 0$ or to $P^* \to \infty$. This results in the fact that $C_\psi = 0$ according to Eq. (44) and $\zeta = 0.7368$ in accordance with Eq. (41a). Inserting these results into Eq. (50) yields:

$$C_{d,1}(\psi \to 0) = \frac{1}{2} \times 0.7368^{5/2} = 0.233$$

On the other hand, for the greatest value of ψ, i.e. $\psi = 0.50$, Eq. (41a) gives $\zeta = 0.7752$ and C_ψ is as $C_\psi = 0.264548$ according to Eq. (44). Therefore, using Eq. (50) the discharge coefficient is such that:

$$C_{d,1}(\psi = 0.50) = \frac{1}{2} \times \left(\frac{1-0.264548^2}{1-\frac{5}{4}\times 0.264548^2}\right)^{5/2} \times 0.7752^{5/2} = 0.2774 \approx 0.277$$

These results allow concluding that in the range of variation of the parameter ψ, that is to say $0 \le \psi \le 0.50$, the discharge coefficient $C_{d,1}$ increases within the extreme values 0.233 and 0.277. Fig. 6 below, plotted in accordance with Eq. (50), shows the variation of the discharge coefficient $C_{d,1}$ with respect to the dimensionless parameter ψ.
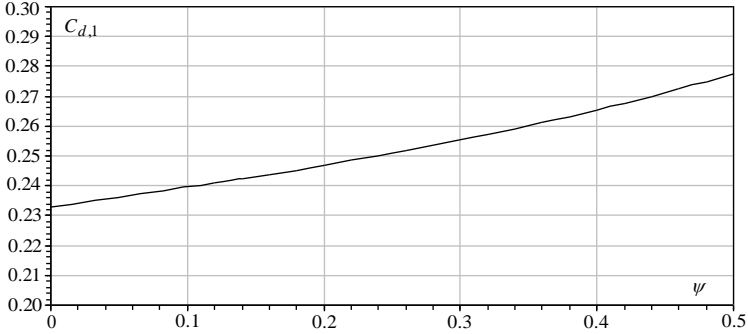
Figure 6: Variation of the discharge coefficient $C_{d,1}$ with respect to ψ according to Eq. (50).

The discharge coefficient can also be expressed in another form. For this, note that Eq. (48) can be written as follows:

$$Q = \frac{1}{2}\sqrt{2g}\,\frac{m\,h_1}{B}\times\frac{B}{h_1}\left(\frac{1-C_{\psi}^2}{1-\frac{5}{4}C_{\psi}^2}\right)^{5/2}\zeta^{5/2}\,h_1^{5/2} \tag{48a}$$

After introducing the dimensionless parameter $M_1 = m\,h_1/B$ and performing some evident simplifications, Eq. (48a) reduces to:

$$Q = \frac{1}{2}\sqrt{2g}\,B\,M_1\left(\frac{1-C_{\psi}^2}{1-\frac{5}{4}C_{\psi}^2}\right)^{5/2}\zeta^{5/2}\,h_1^{3/2} \tag{51}$$

Eq. (51) can be written in the following simple form:

$$Q = C_{d,2}\sqrt{2g}\,B\,h_1^{3/2} \tag{52}$$

where $C_{d,2}$ is the new discharge coefficient which is expressed by the following relationship:

$$C_{d,2} = \frac{1}{2}\,M_1\left(\frac{1-C_{\psi}^2}{1-\frac{5}{4}C_{\psi}^2}\right)^{5/2}\zeta^{5/2} \tag{53}$$

It is easy to demonstrate that Eq. (53) can also be written as follows:

$$C_{d,2} = \frac{1}{2}(1+P^*)\, C_\psi \left(\frac{1-C_\psi^2}{1-\frac{5}{4}C_\psi^2} \right)^{5/2}$$

(54)

It is worth noting that the complete Eqs. (48) and (51) take into account the effect of the approach flow velocity through the quantities in parentheses. As it has been rightly mentioned before, this effect cannot always be neglected at the risk of introducing an undesirable imprecision in the calculation of the flow rate. To our knowledge, this is unfortunately often the case in previous studies relating to the flow measurement.

Experimental validation

The primary goal of this part of the study is to experimentally test Eq. (50) governing the theoretical discharge coefficient. It is a question of knowing if this relation is reliable such as it was expressed or if it will possibly be necessary to correct it in the case where the theoretical and experimental values of the flow are different. If this relation turns out to be faithful and accurate, then Eq. (48) which governs the flow rate would also be. For this, six devices were designed in thin metal and tested in a rectangular channel of 12 meters long, 0.293 meter wide and 0.485 meter deep, fed by a pump providing a maximum flow rate slightly above 30 l/s. The hydraulic system used, made up of the test channel, pump and supply pipe, operates in a closed circuit to ensure permanent flow. Table 2 groups together the characteristics of these devices.

Table 2: Geometric characteristics of the tested devices

Device	Height of the device (cm)	Apex angle $\theta\,(°)$	Crest height P (cm)	Length L of the device (cm)	Channel width B (cm)
1	33	45	10.259	25	29.30
2	33	45	8.232	25	29.30
3	23	60	10.233	25	29.30
4	23	60	8.232	25	29.30
5	21	71	10.268	25	29.30
6	21	71	8.136	25	29.30

The flow rate Q has been varied in the wide range [0.79 l/s; 25.40 l/s] corresponding to measured upstream depths h_1 covering the range [6.52 cm; 31.036 cm]. The crest heights P chosen as well as the upstream depth h_1 measured permit to the relative crest height

$P^* = P/h_1$ varying within the following range $0.292 \leq P^* \leq 1.574$. The dimensionless parameter $M_1 = mh_1/B$ has been varied in the following wide range $0.138 \leq M_1 \leq 0.464$.

Table 3 gives the ranges of the flow rates and upstream depths measured for each of the devices. As it can be seen, 122 couple of values ($Q;h_1$) were obtained during the experimentation, which is a significant sample allowing a correct theoretical analysis. As many values were thus obtained for the experimental and theoretical discharge coefficients $C_{d,Exp}$ and $C_{d,Th}$ where subscripts "*Exp*" and "*Th*" denote "experimental" and "Theoretical" respectively.

Table 3: Range of flow rates and depths used during the testing devices

Device		Number of measurements	Flow rate range (l/s)	Upstream depth range (cm)
$\theta(°)$	P (cm)			
45	10.259	23	$1.76 \leq Q \leq 25.40$	$11.01 \leq h_1 \leq 31.04$
	8.232	19	$1.705 \leq Q \leq 19.81$	$10.87 \leq h_1 \leq 28.18$
60	10.233	20	$1.355 \leq Q \leq 12.64$	$8.69 \leq h_1 \leq 20.72$
	8.232	20	$0.789 \leq Q \leq 12.68$	$7.01 \leq h_1 \leq 20.69$
71	10.268	20	$0.813 \leq Q \leq 12.81$	$6.52 \leq h_1 \leq 19.06$
	8.136	20	$0.89 \leq Q \leq 11.24$	$6.75 \leq h_1 \leq 18.09$

Since the present study is interested in the flow measurement in open channels, it is recommended to experimentally measure the flow rate Q with the greatest possible precision. To meet this requirement, an ultrasonic flowmeter, with an accuracy of around 0.1 to 0.2 l/s, was used. As regards the upstream depth h_1, it is an important parameter in the evaluation of the flow rate. The more accurately the depth h_1 is performed, the more reliable and acceptable the flow rate evaluation. As indicated by Eq. (48) governing the flow rate Q, if a relative error Δ is made on the measurement of the depth h_1, this causes a 2.5Δ relative error on the flow rate evaluation. It is therefore recommended to take measurements of the flow depth using an apparatus as precise as possible. In order to minimize reading errors on the depth h_1, the double precision Vernier point-gauge graduated to $1/10^{th}$ was used with an absolute error of 0.02 mm.

For each test, i.e. for each pair of measured values (Q_{Exp}, h_1), the experimental discharge coefficient of the tested device is calculated according to the following relationship in accordance with Eq. (49):

$$C_{d,Exp} = \frac{Q_{Exp}}{\sqrt{2g}\, m\, h_1^{5/2}} \tag{49a}$$

The experimental discharge coefficients $C_{d,Exp}$ thus calculated will be correlated to the theoretical discharge coefficients $C_{d,Th}$ given by Eq. (50) for knowing to what degree the two coefficients are related. The experimental values of the upstream depth h_1 as well as the flow rates Q are given in tables 4 to 9 in the appendix, for the six tested devices.

Thus, the calculation process of both $C_{d,Exp}$ and $C_{d,Th}$ described above was performed for the six tested devices which finally led to the plotting of their variation curve shown in Fig. 7.
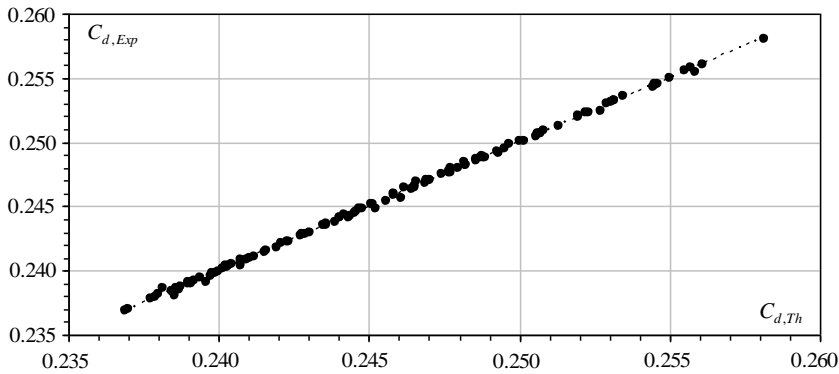

Figure 7: Variation of experimental discharge coefficient $C_{d,Exp}$ according to Eq. (49a) versus theoretical discharge coefficient $C_{d,Th}$ computed using Eq. (50). (- - -) Trend line

Fig. 7 reveals that the experimental and theoretical values of the discharge coefficient align satisfactorily on a curve of linear trend which almost corresponds to the first bisector of equation $C_{d,Exp} = C_{d,Th}$. This important result highlights an outstanding agreement between experiment and theory which proves that the experimental tests were conclusive. Thus, it is quite fair to consider that the theoretical relationship (50) that governs the discharge coefficient is well-founded since it is accurate even though no calibration parameter has been employed. This has the logical consequence to state that Eq. (48) which governs the flow rate is also reliable.

The use of linear least-squares fitting method involving experimental and theoretical data gave the following trend line relationship:

$$C_{d,Exp} = 0.9999\, C_{d,Th} \approx C_{d,Th} \tag{55}$$

Eq. (55) was obtained with a coefficient of determination $R^2 = 0.9992$.

It can be concluded with fulfillment that both the theoretical relationship (48) which governs the flow rate and Eq. (50) which gives the discharge coefficient do not need any correction. It has in fact been observed that the application of Eq. (50) in its current form causes a maximum deviation of less than 0.2% on the calculation of the discharge coefficient. Even better, it was found that in 73.8% of cases, Eq. (50) causes a deviation of less than 0.05%, while in 91.8% of cases the deviation remains less than 0.10%.

CONCLUSION

An in-depth theoretical as well as experimental study was carried out on a flow measurement device in open channels. It is a semi-modular triangular broad-crested weir provided with a crest height *P*. This is the general case of the study recently carried out by the authors on the same device without crest height.

The primary intent of the study is to develop initially an efficient theory capable of deducing the equation governing the flow rate *Q* passing through the device and thus setting down the discharge coefficient relationship. However, the theoretical development foreseen should consider taking into account the effect of the approach flow velocity which is in most cases neglected in previous studies relating to flow measurement. For this, it has been judiciously recommended to rely on the momentum theorem associated with the energy equation. This is, without a doubt, a novelty in the theoretical development of flow metering.

It is intended to design a device of a certain length *L* sufficient to accommodate a control section somewhere inside the triangular gorge faithfully illustrated in Fig. 5 (section c-c). The presence of a control section is the prerequisite for the correct functioning of the device as a flowmeter.

The theory, later confirmed by experimental observations, predicted the change from subcritical flow upstream of the device to supercritical flow inside the gorge. These flow states are clearly recognizable in the photograph of Figs. 3 and 4.

Choosing as reference sections 1-1 and c-c (Fig. 5), the theoretical development, based on the momentum and energy equations, has highlighted the complete form of the relationship governing the discharge while taking into account the effect of the approach flow velocity [Eq. (48)]. This is entirely in accordance with semi-modular devices since the flow rate is both dependent on the geometric characteristics of the device and on the upstream depth of the flow. From the theoretical equation governing the flow rate, it was then easy to deduce that which governs the discharge coefficient [Eq. (50)]. It is this relationship that is of primary interest to this study. As predicted by dimensional analysis, the theoretical relationship of the discharge coefficient confirmed that this one depends on both the effect of lateral and vertical flow contractions reflected by the dimensionless

parameters M_1 and P^* respectively [Eqs. (3) and (9)] grouped together in a single compound parameter ψ [Eq. (8)].

The study continued with the implementation of an intense experimental protocol aimed at verifying the reliability of the theoretical discharge coefficient relationship. For this, six devices of different geometries were designed and tested under appropriate hydraulic conditions (Table 3), having made it possible to collect no less than 122 experimental measurement points of the flow rate and the upstream depth. As many values were obtained for the experimental and theoretical discharge coefficients calculated according to equations (49a) and (50) respectively. The relative errors computed between these two discharges coefficients revealed an almost perfect agreement between the experimental measurements and the corresponding theoretical values (Fig. 7). The use of linear least-squares fitting method involving experimental and theoretical data gave the following trend line relationship obtained with a coefficient of determination $R^2 = 0.9992$:

$$C_{d,Exp} = 0.9999\, C_{d,Th}$$

It is therefore quite obvious that the theoretical relationship governing the discharge coefficient [Eq. (50)] requires no correction. Eq. (50) and therefore Eq. (48) which is closely associated with it can indeed be used with confidence due to their high accuracy. This claim is supported by the fact that the use of Eq. (50) causes, in the worst case, 0.2% maximum deviation between the theoretical and experimental discharges coefficients for the 122 collected measurement points.

Some relevant advantages which characterize the device must be pointed out. It is in particular the triangular shape of the device which has the great advantage of allowing the measurement of both high and low flow rates with excellent accuracy when compared to the well-known rectangular notch. In fact, the accuracy on the measurement of high or low flow rates is the same due to the perfect geometric similarity which the triangular section provides. For the flow measurement in a narrow and deep rectangular approach channel, it is recommended to use such a device provided with a crest height in order to increase the opening angle and thus avoid the harmful effects of surface tension. Finally, it should be noted the ease of implementation of the device which is reduced to only welding thin plates to achieve the simple geometry of the device (Fig. 2).

It should be noted that the disadvantage of the device lies in the fact that it is provided with a crest height in front of which solid debris can accumulate. The device thus designed is not therefore self-cleaning; on the contrary it requires often frequent manual cleaning for eliminating accumulated debris.

REFERENCES

ACHOUR B., AMARA L. (2021). Discharge coefficient for a triangular notch weir theory and experimental analysis, Larhyss Journal, No 46, pp. 7-19.

ACHOUR B., AMARA L. (2021). Discharge measurement in a rectangular open-channel using a sharp-edged width constriction - theory and experimental validation, Larhyss Journal, No 45, pp. 141-163.

ACHOUR B., AMARA L. (2022). Flow measurement using a triangular broad crested weir - theory and experimental validation, Flow Measurement and Instrumentation, Vol. 83, 102088, pp. 1-10.

ACHOUR B., BOUZIANE T., NEBBAR K. (2003). Débitmètre triangulaire à paroi épaisse dans un canal rectangulaire (Première partie), Triangular broad crested flowmeter in a rectangular channel (Part 1), Larhyss Journal, No 2, pp. 7-43, In French.

BOS M.G. (1976). Discharge Measurement Structures, Laboratorium Voor Hydraulica Aan Afvoerhydrologie, Landbouwhogeschool, Report 4, Wageningen, May, The Netherlands.

BOS M.G. (1989). Discharge Measurement Structures, Third Ed., Publication 20, International Institute for Land Reclamation and Improvement, Wageningen, The Netherlands.

CARLIER M. (1998). Hydraulique Générale et Appliquée, General and Applied Hydraulics, Edition Eyrolles, EDF, Department of Studies and Research on French Electricity (EDF), 582p., In French.

HAGER W.H. (1985). Modified Venturi channel, Proceedings, Journal of Irrigation and Drainage Engineering, American Society of Civil Engineers, ASCE, Vol. 111, IR1, pp. 19–35.

HAGER W.H. (1986). Discharge Measurement Structures, Communication 1, Department of Civil Engineering, Federal Polytechnic School of Lausanne, Switzerland.

HENDERSON F.M. (1966). Open Channel Flow, the McMillan Company, New York, N.Y, USA, 522p.

LANGHAAR H.L. (1951). Dimensional Analysis and Theory of Models, John Wiley and Son Ltd, 1st Edition, 166p.

SIA (1926). Contribution à l'étude des méthodes de jaugeage, Contribution to the study of gauging methods, Bulletin 18, Schw. Bureau Wasserforschung, Bern, Switzerland, In French.

TELEDYNE ISCO (2021). Open-Channel Flow Measurement Handbook, https://www.teledyneisco.com/en-us/water-and-wastewater/open-channel-flow-measurement-handbook-request.

VATANKHAH A.R., KHAMISABADI M. (2019). General stage-discharge relationship for sharp-crested power-law weirs: analytical and experimental study, Irrigation and Drainage, Vol. 68, Issue 4, pp. 808–821.

APPENDIX

Table 4: Experimental values of h_1 and Q for the device defined by $\theta = 45°$, $m = 0.41421356$, $P = 0.10259$ m, $B = 0.293$ m

Run	Q_{Exp} (m^3.s^{-1})	h_1 (m)
1	0.00176	0.11008
2	0.001975	0.11538
3	0.002654	0.12962
4	0.003447	0.14362
5	0.005345	0.17042
6	0.00625	0.1811
7	0.00656	0.18462
8	0.006915	0.18836
9	0.007455	0.1941
10	0.00812	0.20046
11	0.0083295	0.20262
12	0.00895001	0.2081
13	0.009458	0.2127
14	0.010242	0.21928
15	0.01081	0.22386
16	0.01128	0.2277
17	0.012215	0.23482
18	0.01418	0.24856
19	0.016795	0.26536
20	0.01748	0.26928
21	0.0195	0.28078
22	0.021585	0.29194
23	0.0254	0.31036

Table 5: Experimental values of h_1 and Q for the device defined by $\theta = 45°$, $m = 0.41421356$, $P = 0.08232$ m, $B = 0.293$ m

Run	Q_{Exp} (m^3.s^{-1})	h_1 (m)
1	0.001705	0.10868
2	0.001977	0.11524
3	0.002575	0.12784
4	0.002961	0.13504
5	0.00441	0.15784
6	0.00545	0.17144
7	0.00637	0.18214
8	0.006855	0.18752
9	0.0074501	0.19354
10	0.00818	0.2007
11	0.00895	0.20788
12	0.00955	0.21314
13	0.01018	0.2184
14	0.011604	0.2297
15	0.012478	0.23628
16	0.01407	0.24736
17	0.01548	0.25654
18	0.0175	0.26884
19	0.01981	0.28184

Table 6: Experimental values of h_1 and Q for the device defined by $\theta = 60°$, $m = 0.57735027$, $P = 0.10233$ m, $B = 0.293$ m

Run	Q_{Exp} (m³.s⁻¹)	h_1 (m)
1	0.001355	0.08688
2	0.001571	0.09214
3	0.001803	0.09724
4	0.00198333	0.10096
5	0.002286	0.10678
6	0.002452	0.10976
7	0.002821	0.11598
8	0.0031825	0.12156
9	0.003672	0.12856
10	0.004025	0.13326
11	0.00448	0.1389
12	0.005032	0.14536
13	0.006712	0.16252
14	0.00704	0.16552
15	0.00764	0.1708
16	0.00813	0.175
17	0.008675	0.1794
18	0.00928	0.1841
19	0.010282	0.19152
20	0.01264	0.20716

Table 7: Experimental values of h_1 and Q for the device defined by $\theta = 60°$, $m = 0.57735027$, $P = 0.08232$ m, $B = 0.293$ m

Run	Q_{Exp} (m^3.s^{-1})	h_1 (m)
1	0.0007896	0.07014
2	0.001392	0.08774
3	0.001501	0.09038
4	0.001839	0.0979
5	0.002038	0.1019
6	0.002282	0.10658
7	0.002692	0.11372
8	0.002983	0.11834
9	0.00421	0.13534
10	0.00445	0.1383
11	0.005695	0.15222
12	0.00603	0.15562
13	0.00643	0.1595
14	0.00687	0.16364
15	0.00755	0.16972
16	0.00822	0.1753
17	0.00908	0.18218
18	0.01019	0.19038
19	0.01131	0.1981
20	0.012682	0.20694

Table 8: Experimental values of h_1 and Q for the device defined by $\theta = 71°$, $m = 0.71329307$, $P = 0.10268$ m, $B = 0.293$ m

Run	Q_{Exp} (m^3.s^{-1})	h_1 (m)
1	0.000813	0.06522
2	0.0011625	0.07512
3	0.001361	0.07994
4	0.00161667	0.08554
5	0.00189	0.09098
6	0.002157	0.0958
7	0.0024895	0.10134
8	0.002935	0.1081
9	0.003372	0.1141
10	0.003792	0.11942
11	0.004015	0.12214
12	0.004562	0.12832
13	0.004795	0.13082
14	0.006042	0.14306
15	0.007254	0.15348
16	0.00868	0.16442
17	0.01005	0.1739
18	0.01186	0.18522
19	0.01238	0.1882
20	0.01281	0.19064

Table 9: Experimental values of h_1 and Q for the device defined by $\theta = 71°$, $m = 0.71329307$, $P = 0.08136$ m, $B = 0.293$ m

Run	Q_{Exp} (m^3.s^{-1})	h_1 (m)
1	0.0008901	0.06752
2	0.00118333	0.07558
3	0.001363	0.07988
4	0.001612	0.08534
5	0.001828	0.08964
6	0.002118	0.09498
7	0.002597	0.10286
8	0.002842	0.10654
9	0.00321	0.11172
10	0.003714	0.11824
11	0.00442	0.12648
12	0.004825	0.13086
13	0.00553	0.13794
14	0.00606	0.14286
15	0.00651	0.14686
16	0.007116	0.15198
17	0.007915	0.1583
18	0.00856	0.16308
19	0.00949	0.1696
20	0.01124	0.18086